Composites Part B 199 (2020) 108259

Contents lists available at ScienceDirect

Composites Part B

journal homepage: www.elsevier.com/locate/compositesb

Scalable synthesis of robust and stretchable composite wound dressings by dispersing silver nanowires in continuous bacterial cellulose

Yizao Wan [a,b,c], Shanshan Yang [a], Jie Wang [a], Deqiang Gan [a], Miguel Gama [d], Zhiwei Yang [a], Yong Zhu [e], Fanglian Yao [e], Honglin Luo [a,b,c,*]

[a] Institute of Advanced Materials, East China Jiaotong University, Nanchang, 330013, China
[b] Jiangxi Key Laboratory of Nanobiomaterials, East China Jiaotong University, Nanchang, 330013, China
[c] School of Materials Science and Engineering, Tianjin University, Tianjin, 300072, China
[d] Centro de Engenharia Biológica, Universidade Do Minho, Campus de Gualtar, P 4715-057, Braga, Portugal
[e] Department of Polymer Science and Key Laboratory of Systems Bioengineering of Ministry of Education, School of Chemical Engineering and Technology, Tianjin University, Tianjin, 300072, China

ARTICLE INFO

Keywords:
Wound dressing
Bacterial cellulose
Silver nanowire
Antibacterial activity

ABSTRACT

While silver nanoparticles are widely used to endow materials with antibacterial activity, silver nanowires (AgNWs) have not attracted much attention. Herein, the composites of bacterial cellulose (BC) and AgNWs were prepared through a novel step-by-step *in situ* biosynthesis which retains the three-dimensional network of BC. The results of water vapor permeability, water uptake rate, and water retention rate showed that the BC/AgNW wound dressings could absorb wound skin exudates and maintain moisture environments. Furthermore, the BC/AgNW dressings were robust and stretchable. More importantly, the BC/AgNW dressings exhibited sustained release of Ag^{+}. The results from animal tests indicated that the BC/AgNW dressing with 38.4 wt% AgNWs exhibited higher expression levels of cytokeratin-10 and integrin-β4, greater proliferation of keratinocytes and formation of epithelial tissues and greatly improved skin regeneration over the bare BC. We propose that the integrated nanofibrous structure and the excellent and sustained antibacterial activity of AgNWs are responsible for the excellent *in vivo* wound healing ability and biocompatibility. These results suggest that the BC/AgNW composites have promising application as wound dressings.

1. Introduction

Since its discovery in 1880s by A. J. Brown [1], bacterial cellulose (BC) has attracted much attention during the last decades and its potential applications cover a wide variety of areas from the earliest skin substitutes for burns and ulcers, food additives, cosmetics, facial masks, and papers to the sophisticated products of artificial cartilage, bone, heart valve prosthesis, artificial blood vessels, cornea and so on [2,3]. Such broad applications of BC are attributable to its striking physical and mechanical characters, including high purity, hydrophilicity, crystallinity, biocompatibility, ultrafine fiber diameter (20–100 nm), high water holding capacity, high mechanical properties, broad chemical and physical modifying ability, shapeability, and nano-scaled three-dimensional (3D) network structure [4]. Although numerous materials have been developed to make wound dressings [5–10], BC is also a suitable material for wound dressings since it can provide a moist environment which is beneficial for healing [11] and biodegradability is not mandatory in wound dressings. Although providing an effective biological barrier to the wound, the fact that BC has no antibacterial activity limits its applications in clinics. In this context, much effort has been made to endow it with antibacterial activity. To date, many papers regarding BC antibacterial wound dressings have been published [12–15], among which those with silver nanoparticles (AgNPs) are the most common [13,14] although other agents such as chitosan [16], ε-polylysine nanocoatings [17], amoxicillin [15], to name a few, have also been employed. Usually, the *in situ* metallization technique is employed to introduce AgNPs onto BC, simply by immersing BC in a silver nitrate solution followed by reducing the absorbed silver ions (Ag^{+}) to metallic AgNPs under the reduction action of sodium borohydride. The AgNPs-loaded BC exhibit strong antibacterial activity against gram-negative *Escherichia coli* (*E. coli*) and gram-positive *Staphylococcus aureus* (*S. aureus*) [18].

* Corresponding author. Institute of Advanced Materials, East China Jiaotong University, Nanchang, 330013, China.
E-mail address: hlluotju@126.com (H. Luo).

https://doi.org/10.1016/j.compositesb.2020.108259
Received 28 February 2020; Received in revised form 25 June 2020; Accepted 28 June 2020
Available online 31 July 2020
1359-8368/

As an alternative candidate, silver nanowires (AgNWs) have also gained growing attention in the field of antibacterial agents [19]. It is hypothesized that, unlike AgNPs, i) AgNWs may have a reinforcing effect due to their higher length-to-diameter ratio and thus stronger antibacterial BC wound dressing may be obtained; ii) AgNWs do not block pores, which are important to maintain air circulation; iii) AgNWs do not experience rapid release of Ag^+ and thus a more sustained release and improved biocompatibility is expected. However, the studies on BC/AgNW composites are very limited. This is due to the difficulty in dispersing AgNWs throughout the BC network, which is much more difficult compared with AgNP-loaded BC dressings which are realized by solution immersion. In general, two methods are used for adding nanofillers to BC matrix, namely mechanical mixing and *in situ* biosynthesis [20]. The first method breaks the integrated structure of BC while the second one cannot achieve uniform distribution of AgNWs in BC due to their large fiber length. The pioneering work conducted by Lv et al. reported a BC/AgNW composite thin film which was fabricated by vacuum filtration [21]. Using this method, the AgNWs are concentrated on the top of BC membrane, leading to a bilayered structure. Therefore, to achieve uniform distribution of AgNWs in the entire BC network is still a challenge.

In this work, inspired by our previous work which uniformly dispersed graphene [22] and graphene oxide [23] in the BC matrix, we report for the first time novel BC/AgNW composite dressings which were prepared by the step-by-step *in situ* biosynthesis [20,22,24,25]. It is hypothesized that this novel method may lead to a new BC/AgNW dressing that will possess uniformly dispersed AgNWs throughout the BC matrix and exhibit good mechanical properties and favorable biocompatibility.

2. Materials and methods

2.1. Materials

Commercially available AgNW suspension was purchased from VIGON Technologies (Hefei, China). Reagents for biosynthesis of BC included acetic acid, glucose, tryptone, yeast extract, and disodium phosphate. All chemicals were provided by Acros (New Jersey, USA) and used as received with no purification. The bacterial strain for BC production was *Komagataeibacter xylinus* X-2, from Tianjin University of Science and Technology, Tianjin, China.

2.2. Preparation of BC and BC/AgNW dressings

A BC pellicle was prepared by static culture according to previously described procedure [26]. The cultured BC pellicle became the substrate for subsequent BC/AgNW pellicles preparation using the step-by-step *in situ* biosynthesis [20,22,24,25]. AgNW-containing culture media were prepared by adding AgNW suspension (5 mg mL^{-1}) to the culture medium at varying volume ratios of 10 : 1, 10 : 3, and 10 : 4.5, followed by vigorous stirring for 1 h, similar to our previous work [20,24,25] (a AgNW suspension was prepared, rather than graphene oxide). The schematic diagram of the preparation procedures is displayed in Fig. 1. The processes include repeated spraying and *in situ* growth of BC until a predetermined thickness (0.5–2.0 mm depending on the usage) is achieved. The harvested BC/AgNW pellicles were boiled in NaOH solution to remove the bacterial cells. The pellicles were then thoroughly rinsed in deionized water. The obtained pellicles were freeze-dried for 24 h, yielding BC/AgNW dressings, which are named BC/AgNW-1, BC/AgNW-2, and BC/AgNW-3, corresponding to AgNW suspension to culture medium ratios of 10 : 1, 10 : 3, and 10 : 4.5, respectively.

2.3. Characterization

Scanning electron microscope (SEM, SU8010, Japan) was used to observe the morphology of the composites. The average fiber diameter was determined by measuring at least 100 fiber segments, similar to our previously reported method [27]. Similarly, at least 200 pores were selected to measure the pore size [28]. Atomic force microscopy (model 5500, Agilent, USA) images were recorded under the tapping mode. An Xpert Pro MPD X-ray diffractometer (XRD) was used to assess their crystal structure with Cu-K_α radiation ($\lambda = 154$ nm). Fourier transform infrared spectroscopy (FTIR, Spectrum one, PerkinEler) and X-ray photoelectron spectroscopy (XPS, AXIS Ultra DLD, Japan) were conducted to determine the surface chemistry. Thermogravimetric analysis (TGA) was performed with a thermal analyzer (PerkinElmer Pyris 1, USA) from room temperature to 600 °C at a heating rate of 10 °C min^{-1} under N_2 flow (100 mL min^{-1}).

The contact angle was determined with a contact angle goniometer (CA, JGM-360B, Chengde Chenghui Testing Machine Co. Ltd. Chengde, China) with a 5 μL water droplet. Brunauer–Emett–Teller (BET) surface area of BC and BC/AgNW dressings was evaluated from nitrogen adsorption isotherms at 77 K with a surface area analyzer (NOVA 2200e).

The tensile properties of BC/AgNW dressings (in wet state) were characterized with a MUF-1050 micro-electromagnetic fatigue tester (Tianjin Care Measure & Control Co. Ltd. Tianjin, China). The measurements were conducted at a 5-mm min^{-1} strain rate (room temperature, 25 °C, 65% relative humidity). The tensile tests were performed on rectangular specimens with a size of 20 mm × 5 mm × 1 mm. The

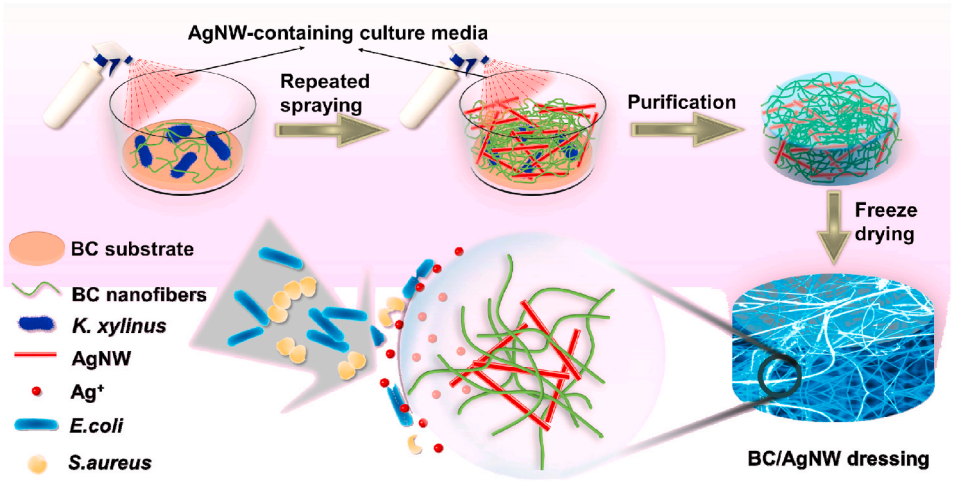

Fig. 1. Schematic illustration of BC/AgNW dressing preparation.

testes were repeated at least 5 times to calculate the means and standard deviations.

Based on Archimedes' principle, the total porosity was determined from the liquid displacement method [6]:

$$Porosity(\%) = \frac{M_2 - M_3 - M_s}{M_1 - M_3} \times 100\% \quad (1)$$

where M_1 and M_2 represent the weights of two specific gravity bottles which contained ethanol and BC/AgNW dressings, respectively; M_3 means the weight of the bottle and remaining ethanol after removing the BC/AgNW dressings; M_s is the dry weight of the BC/AgNW dressings before submerged into ethanol.

Water uptake ability (W_A) was quantified as follows. Briefly, the freeze-dried dressings were weighed (W_0) followed by submerging in SBF (simulated body fluid) for a predetermined duration of time (20–140 min). The fluid-filled dressings were subsequently gently transferred with tweezers to a Petri dish, where the dressings were allowed to stand for 1 min to allow the removal of excess liquid on the surface. The dressings were then weighed (W_t) to calculate the water uptake ability, W_A, from Equation (2) [29].

$$W_A = \left[\frac{W_t - W_0}{W_0}\right] \times 100\% \quad (2)$$

The water retention rate (W_R) was measured by keeping dressings in the conditions of 25 °C and relative humidity of 65% for different time durations. The W_R was calculated using the equation [30]:

$$W_R = \left[\frac{W_t - W_d}{W_w - W_d}\right] \times 100\% \quad (3)$$

where W_d is the weight of dried dressings, W_w is the initial weight of the wet dressings, and W_t is the weight of dressings after conditioning for t h.

The water vapor transmission rate (*WVP*) describes the water permeability of a film during a predetermined time period. The *WVP* of BC/AgNW dressings was determined at 20 °C using glass vials with an opening covered with BC/AgNW dressings (hydrogel, circular shape, diameter 30 mm, thickness 0.5 mm) according to previously reported method [31]. The glass vials containing 10 mL of deionized water were put in a desiccator at 20 °C for 7 h, where silica gel was used to maintain a constant low humidity. The water vapor can penetrate through the exposed dressings. At regular intervals during the 7 h, the weights of the watering-containing vials were measured. The *WVP* (g m^{-1} h^{-1} Pa^{-1}) can be calculated using the equation [32]:

$$WVP = \frac{S \times d}{A \times \Delta P} \quad (4)$$

where S (g h^{-1}) is the rate of water evaporation through the dressings as determined by the slope of the graph with the weight of vials (g) vs time (h); d and A are the thickness (m) and the area (m^2) of the dressings, respectively. Δp represents the difference in water vapor pressure across the dressings (2.33 kPa at 20 °C) [32].

Release of Ag^+ was tested using freeze-dried circular dressings with a diameter of 15 mm. Dressings were immersed in 50 mL of the deionized water for different periods at 37 °C. The suspending fluids were then analyzed for Ag^+ by an inductively coupled plasma optical emission spectrometer (ICP-OES, Optima 5300DV, PerkinElmer, Shelton, USA).

2.4. Antibacterial activity assay

S. aureus (ATCC 25923) and *E. coli* (ATCC 8739), two typical Gram-positive and negative bacteria, respectively, were used to determine the antibacterial profiles of various dressings, which were quantified with both disc-diffusion and colony forming unit (CFU) methods.

2.4.1. Disc-diffusion method

The antibacterial properties were evaluated with a disk diffusion test where the zone of inhibition (halo width) was measured. One-hundred microliter *E. coli* or *S. aureus* suspension was evenly spread on Luria-Bertani (LB) agar plates. Subsequently, circular BC/AgNW dressings (15 mm in diameter) were placed onto the LB agar plates and incubated overnight at 37 °C. The halo width was determined with ImageJ software.

2.4.2. CFU method

Twenty-four-well culture plates were filled with 500 μL of LB medium containing 10^{11} CFU mL^{-1} of *E. coli* or *S. aureus*. The BC/AgNW dressings were then placed in the wells and incubated at 37 °C. Subsequently 100 μL of the medium was removed from the well and spread onto fresh LB agar plates to incubated at 37 °C for 24 h. The CFU values were used to calculate the antibacterial ratio (A_r) with Equation (5):

$$A_r = \left[\frac{C_b - C_e}{C_e}\right] \times 100\% \quad (5)$$

where C_b and C_e represent the colony counts of blank and experimental groups, respectively.

2.4.3. Fluorescent microscopy analysis

Bacterial fluorescent staining live/death assay was performed. *S. aureus* and *E. coli* suspensions containing 10^6–10^7 CFU mL^{-1} were used. The bacteria were incubated with dressings at 37 °C for 24 h. The mixture was stained with 4′,6-diamidino-2-phenylindole (DAPI) following the instructions from the DAPI staining kit and imaged with a fluorescence microscope (Nikon TS2, Japan).

2.5. Biocompatibility testing

To evaluate the biocompatibility of the AgNW-containing dressing, the mouse embryonic fibroblast cell line (NIH-3T3) were selected to conduct the Cell Counting Kit-8 (CCK-8) assay. NIH-3T3 cells were maintained in minimal essential medium (MEM) with fetal bovine serum. The dressings were sterilized, soaked in MEM for 12 h, and incubated in a 24-well plate for 1, 2, and 3 days under the standard cell culture condition. Then, the dressings with adsorbed cells were transferred to another 24-well plate, followed by the addition of 50 μL of CCK-8 reagent and 500 μL of culture medium per well, followed by incubation for 4 h (in darkness) under the standard cell culture condition. Subsequently, the culture medium was collected and poured into to a 96-well plate to determine the absorbance at a wavelength of 450 nm.

2.6. In vivo wound healing ability

2.6.1. Animal experiments

A total of 48 male Institute of Cancer Research (ICR) mice (8-week old, 22–25 g) were provided by the Experimental Animal Center of Nanchang University, Nanchang, China. All animal experiments were conducted in accordance with the ethical guidelines approved by the Animal Use and Care Administrative Advisory Committee of the East China Jiaotong University. Before the creation of wounds, anaesthetization was achieved with 5% chloral hydrate (Merck, Germany) given intraperitoneally. The dorsal region skin of mice was depilated using an electric shaver and then disinfected with 70% alcohol. The back of the mice was shaved and circular excisional full-thickness wounds with diameter of 15 mm were created. The mice were divided into three groups (16 mice each): BC group, wounds in each animal were covered with BC dressing; BC/AgNW-3 group, covered with BC/AgNW-3 dressing; control group, wounds in each mouse received no treatment. Each mouse was kept in separate cages with complete access to food and water. Wound healing was monitored by optical microscope on certain time points (3rd, 6th, 9th, and 12th days). Wound healing rate (*WHR*) was expressed as $WHR = (A_0 - A_f)/A_0$. The initial area (A_0) represents the area measured at the time of the surgery (day 0) while the final area (A_f)

is the area measured at the time of euthanasia (day 3, 6, 9, and 12).

2.6.2. Histological analysis

The wound healing process was also observed at a histological level. At predetermined times, samples of wounds and surrounding tissues were collected from the animals on the 3rd and 12th post-operative days. The excised tissue was fixed with 4% formaldehyde and embedded in paraffin, which were then sliced into 5.0 μm-thick histological sections, affixed onto glass slides, and stained with Hematoxylin and Eosin (HE) dye for histological analysis. The stained samples were visualized under an optical microscope (Nikon TS2, Japan).

2.6.3. Immunohistochemistry

For immunohistochemistry staining, the sections, affixed on the slides, were deparaffinized, treated with antigen retrieval solution, and incubated with 5% normal donkey serum for 1 h to minimize nonspecific staining. The sections were incubated with primary antibodies overnight at 4 °C, with secondary antibodies for 2 h at 37 °C, then counterstained with DAPI for 10 min at 18–21 °C, followed by observation under the aforementioned optical microscope.

2.7. Statistical analysis

Statistical analysis was accomplished with the SPSS Statistics (v20) and a one-way ANOVA. Results with p-values of less than 0.05 were considered statistically significant. Data were expressed as the means ± standard deviations.

3. Results

3.1. Morphology, structure, and physiochemical properties

Prior to morphology observation, TGA was conducted and the results show the contents of AgNWs in BC/AgNW-1, -2, -3 dressings are 11.2%, 30.0%, and 38.4% (dry weight), respectively (Fig. S1, Supplementary Material).

Fig. 2 presents the digital images and SEM images of bare BC, AgNWs, and BC/AgNW dressings. Fig. 2a demonstrates the difference in color among the dressings due to their different AgNW contents. Fig. 2b is a representative SEM image of AgNWs and Fig. 2c shows a typical SEM image of BC. As shown in Fig. 2d–f, it is difficult to distinguish BC nanofibers from AgNWs under SEM observation as they have similar diameter (Fig. 2g and Fig. S2, Supplementary Material) and appreance. The EDS result (Fig. S3, Supplementary Material) confirms the uniform distribution of AgNWs in BC/AgNW-3. Fig. 2h demonstrates that the as-prepared BC/AgNW dressings are strong, flexible, and stretchable, which make them suitable as a clinical dressing product.

To determine the crystal and chemical structures of BC/AgNW dressings, XRD, FTIR, and XPS examinations were conducted. Fig. 3a reveals three dominant diffraction peaks in the XRD pattern of BC, which

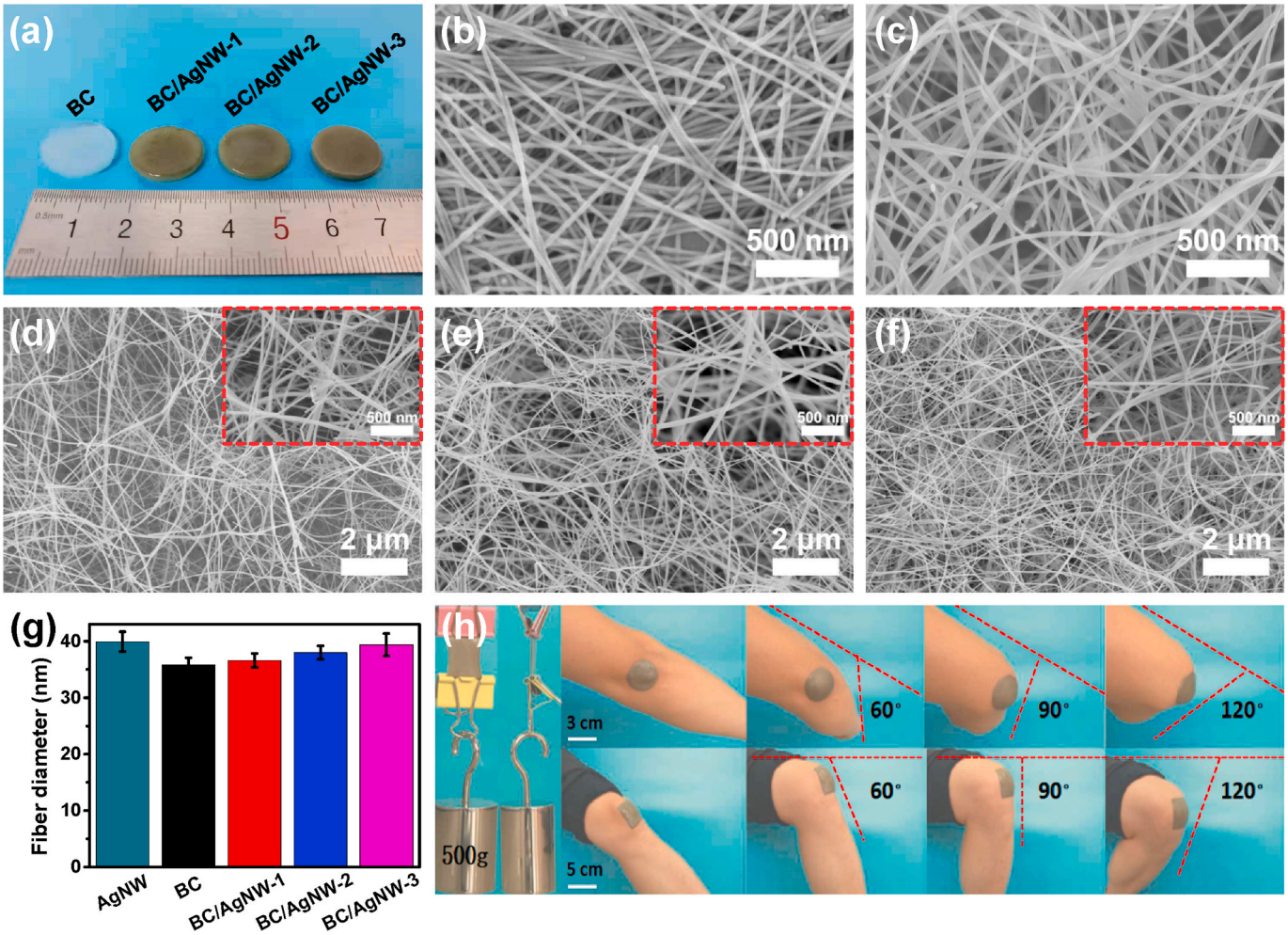

Fig. 2. (a) Digital images of BC and BC/AgNW dressings. (b–f) SEM images of AgNWs (b), BC (c), BC/AgNW-1 (d), BC/AgNW-2 (e), and BC/AgNW-3 (f) dressings. Insets in d, e, and f show higher magnification images. (g) Average fiber diameter of AgNWs, BC, and BC/AgNW dressings. (h) Digital images showing the robustness and excellent stretchability and flexibility of the BC/AgNW dressings.

are located at 2θ = 14.7°, 16.0°, and 22.7°, which are typical patterns of cellulose I [24]. In addition, in the spectra of BC/AgNW dressings, five typical diffraction peaks associated with AgNW crystals are detected at 2θ = 38.1°, 44.2°, 64.5°, 77.3°, and 81.4°, which are diffractions of (111), (200), (220), (311), and (222) planes, respectively [33]. The XRD result confirms the formation of BC and Ag composites.

To determine whether there is any interaction between AgNWs and BC, FTIR analysis was conducted (Fig. 3b). The bands at 1057 and 1112 are due to C–O stretching vibration and the peak at 1163 cm^{-1} corresponds to the C–O–C stretching vibration [34]. The band at 1617 cm^{-1} can be assigned to C═O [35]. An additional peak at 1558 cm^{-1} in the BC/AgNW dressings' spectra results from the hydrogen bonding interaction between BC and AgNWs [35].

XPS analysis was also conducted (Fig. 3c–e). The wide-scan spectrum shows the presence of Ag, C, and O elements (Fig. 3c), agreeing with the EDS result. Fig. 3d displays two peaks in the Ag 3d region, corresponding to Ag $3d_{5/2}$ and Ag $3d_{3/2}$, belonging to metallic silver, consistent with several previous studies [36,37]. Fig. 3e reveals the right shift of O 1s for BC/AgNW-3 as compared to bare BC, which indicates the possible hydrogen bonding between –OH groups in BC and the carbonyl groups of PVP on AgNWs [38], agreeing with the FTIR result.

The mechanical properties of BC/AgNW dressings were measured. The tensile stress-strain curves show similar trend and the maximum stress increases with the content of AgNWs (Fig. 4a). The quantitative results in Fig. 4b demonstrate the same pattern. The highest tensile strength (1.56 MPa) and modulus (2.88 GPa) are observed in BC/AgNW-3 while its strain at break (44%) is comparable to other samples including BC dressing (38.8%–43.8%). The improved strength and modulus upon the addition of AgNWs are due to the entanglement between continuous BC nanofibers and discontinuous AgNWs and hydrogen bonding between them.

Nitrogen adsorption-desorption experiments were performed to examine the surface area. As shown in Fig. S4 (Supplementary Material), BC and BC/AgNW dressings show typical type IV isotherms with type H3 hysteresis loop according to BDDT classification [39]. It is noted that the Brunauer-Emmet-Teller (BET) specific surface area of BC is 322 $m^2\ g^{-1}$, which decreases to 143 $m^2\ g^{-1}$ for BC/AgNW-3, suggesting that incorporation of AgNWs leads to reduction in specific surface area. Furthermore, the pore size and porosity were determined and presented in Figs. S5 and 6 (Supplementary Material), respectively, which demonstrate that the average porosity and pore size decrease with the content of AgNWs.

The BC/AgNW dressings were further characterized to determine their water uptake ability (W_A) and water retention ratio (W_R). W_A is of great importance in wound dressings which controls wound exudates and maintains moist environment on the wounds. As shown in Fig. 5a, the W_A of both BC and BC/AgNW dressings increases with soaking time. For all samples, a rapid increase in W_A is observed during the first 20 min, and it slows down afterwards. It is believed that the BC/AgNW dressings absorb water through two ways, namely i) chemical route due to the high water affinity of BC and ii) physical route due to the pores within the 3D network and low water contact of BC, which generates the Laplace pressure and capillary force that drives the water into the pores [18]. Note that the BC/AgNW dressings uptake less water than BC and the W_A value of BC/AgNW decreases with the AgNW content due to their lower porosity (Fig. S6, Supplementary Material) and larger water contact angle (Fig. S7, Supplementary Material). It is worth to mention that the W_A values of all BC/AgNW dressings are still at a high level, which are over 6000% after immersing in the deionized water for 140 min. Such a good absorption property of BC/AgNW dressings enables them to absorb a great deal of exudate, which makes them potential wound dressings.

Similarly, the ability to control the water loss at an ideal rate is also important for wound dressings [40]. Therefore, the W_R of various BC/AgNW dressings was estimated (Fig. 5b). As expected, the W_R of BC and BC/AgNW decreases with exposure time. It is noted that the BC/AgNW-3 still keeps 35.7% water after 12 h and the value decreases to 13.7% at 24 h. These values are higher compared to some previously

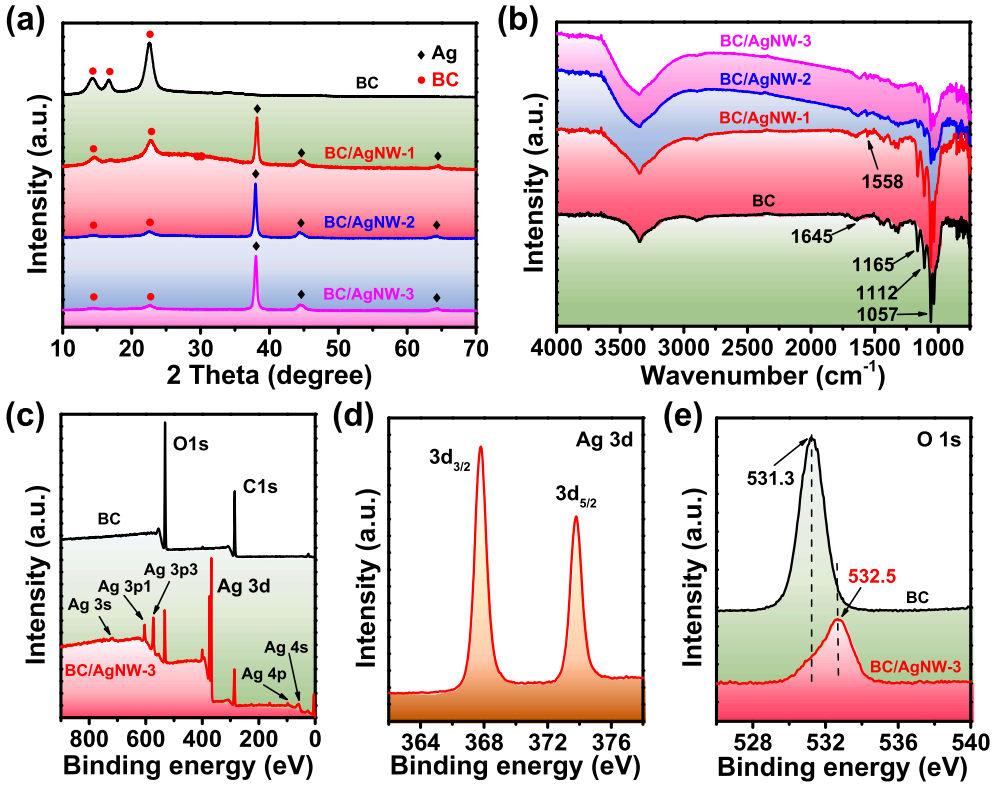

Fig. 3. (a) XRD patterns of BC/AgNW dressings. (b) FTIR spectra of BC/AgNW dressings. (c) Full-scan XPS spectrum of BC and BC/AgNW-3 dressings. (d) XPS spectrum of the Ag 3d region of BC/AgNW-3 dressing. (e) High-resolution spectra of O 1s of BC and BC/AgNW-3 dressings.

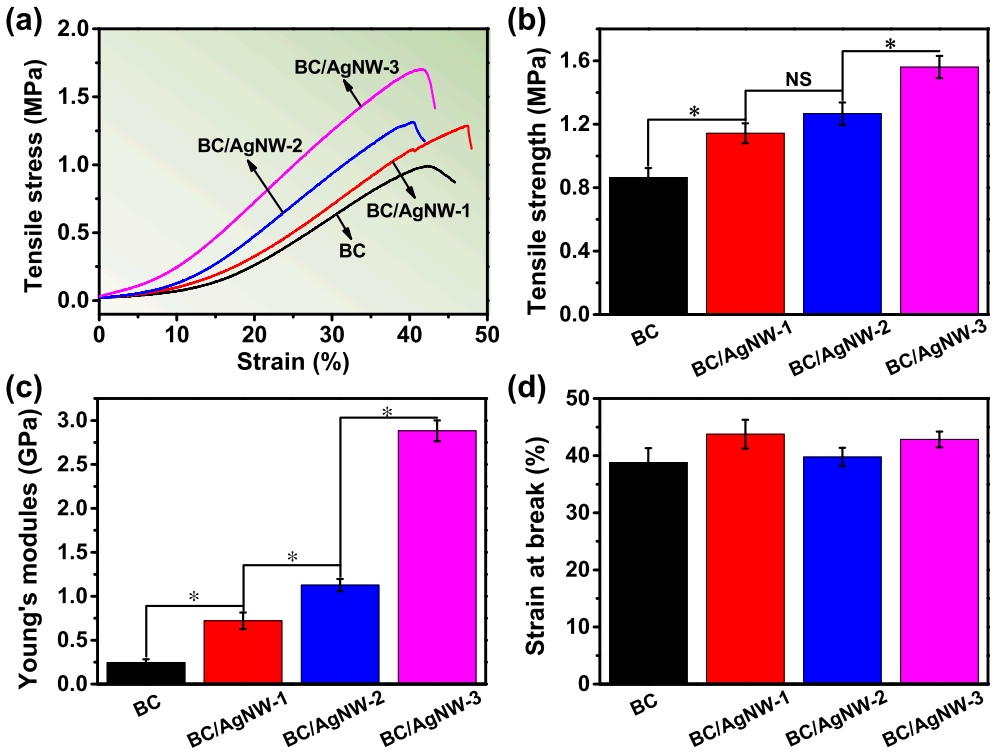

Fig. 4. Mechanical properties of BC/AgNW dressings. (a) Stress-strain curves. (b) Tensile strength. (c) Tensile modulus. (d) Strain at break. *$p < 0.05$, n = 5. NS means insignificant, $p > 0.05$.

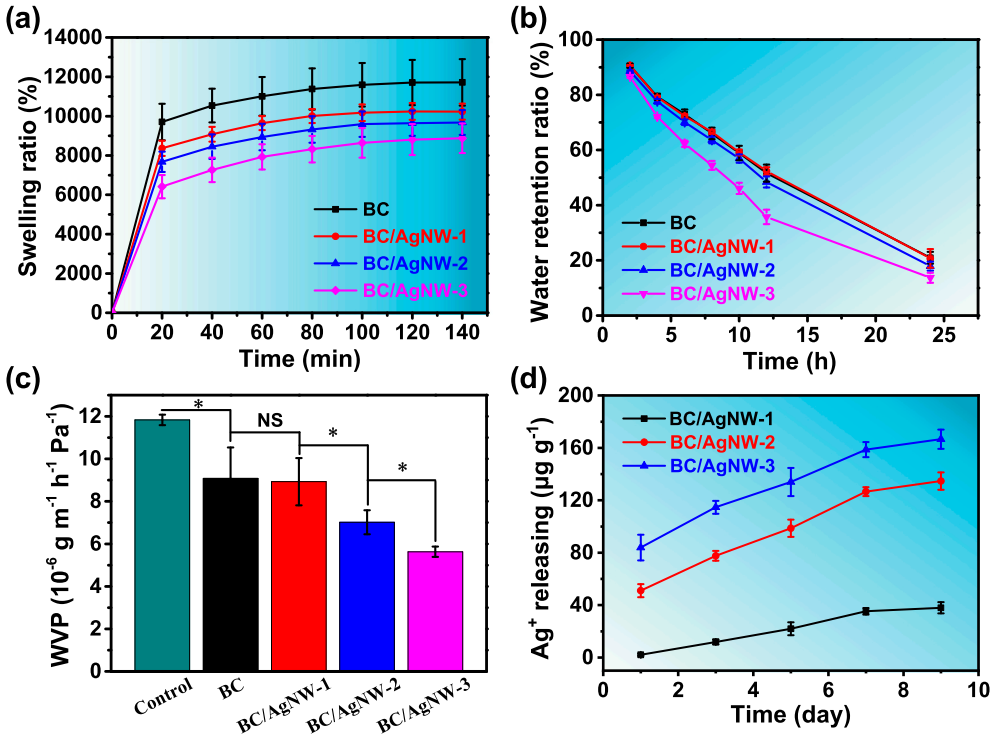

Fig. 5. Water uptake (a), water retention rate (b), and water vapor permeability (WVP) (c) of BC/AgNW dressings. (d) Release profiles of Ag^+ from BC/AgNW dressings. *$p < 0.05$, n = 4. NS means insignificant, $p > 0.05$.

reported materials such as maghemite/cellulose nanocomposite membrane which kept 10% water at 7 h [41]. The higher W_R of BC/AgNW dressings can keep the wound moist for a longer time, which benefits healing.

As seen in Fig. 5c, the WVP of bare BC dressing is 9.1 × 10^{-7} g $m^{-1}h^{-1}Pa^{-1}$ while BC/AgNW-3 dressing shows a WVP of 5.6 × 10^{-7} g $m^{-1}h^{-1}Pa^{-1}$, demonstrating a decreasing trend with the content of AgNWs [32].

Fig. 5d shows the Ag^+ release behavior starting from 24 h since Ag^+ concentration was too low to detect (below the lower limit of the machine) before 24 h. The approximate linear lines demonstrate that BC/AgNW dressings release Ag^+ quite stably.

3.2. Antibacterial activity

The antibacterial activities of BC/AgNW dressings against gram-positive *S. aureus* and gram-negative *E. coli* were measured by disc diffusion and colony forming unit (CFU) methods. The halo test results are shown in Fig. 6a. It is seen that bare BC dressing shows no halo circle for *S. aureus* and *E. coli*, as expected. All BC/AgNW dressings display distinct halos around the circular dressings, due to the release of Ag^+. In addition, the antibacterial activities against *S. aureus* and *E. coli* increase with the content of AgNWs.

To further quantify the antibacterial activities, CFU method was used (Fig. S8 and Table S1, Supplementary Material). It is found that, after only 6 h of incubation, the percentage reduction of *S. aureus* is larger than 80% for all samples, approaching 100% for BC/AgNW-3. The fluorescence microscope images (Fig. 6b) reveal the same trend, consistent with the disc diffusion and CFU results. Interestingly, the antibacterial activities of BC/AgNW dressings against *E. coli* is weaker than *S. aureus*. Such result was also reported by other researchers, which is due to the fact that the cell wall of the Gram-negative bacteria consisting of lipids, proteins and lipopolysaccharides can provide effective protection against biocides whereas the Gram-positive bacteria do not have lipopolysaccharides [42]. Overall, BC/AgNW dressings exhibit excellent antibacterial activities against *S. aureus* and *E. coli*.

The morphologies of *S. aureus* and *E. coli* cells grown on the BC/AgNW-3 dressing were observed by SEM (Fig. 6c). The *S. aureus* cells on BC dressing are typically round-shaped and the *E. coli* cells are rod-shaped and both types of cells exhibit smooth intact cell walls. The cell numbers of *S. aureus* and *E. coli* reduce markedly after culture with BC/AgNW-3 and collapsed, wrinkled, and damaged membranes are noted, suggesting the significant role of BC/AgNW-3 in damaging *S. aureus* and *E. coli*.

3.3. Biocompatibility of BC/AgNW dressings

CCK-8 assay was conducted to assess the cell viability of BC/AgNW dressings by using NIH-3T3 cells which were incubated on the sample surfaces for 1, 2, and 3 days. Fig. 7a demonstrates a lack of significant difference in cell viability between bare BC and BC/AgNW dressings at day 2 and 3, although there is significant difference between BC and BC/AgNW-3 on day 1 ($p < 0.05$), indicating their good biocompatibility and thus being promising biomedical material for wound dressing application.

The NIH-3T3 cells cultured on BC/AgNW dressings for 1, 2, and 3 days were investigated by fluorescent microscopy (Fig. 7b). There is little difference in cell growth and morphology between BC and BC/Ag

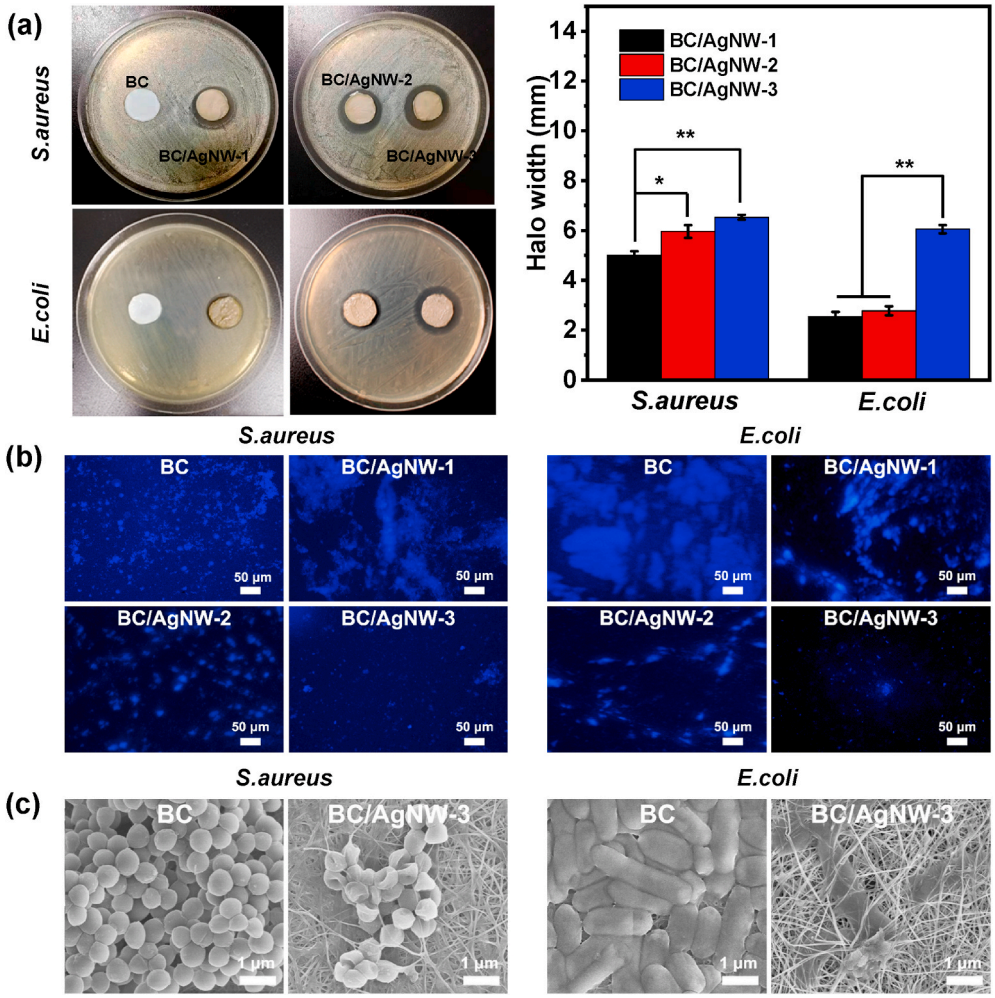

Fig. 6. Antibacterial activity of BC/Ag dressings. (a) Digital images and halo width of the inhibition zone of BC/Ag dressings against *S. aureus* and *E. coli*. (b) Fluorescence microscopy images of adherent *S. aureus* and *E. coli* on the surfaces of BC/Ag dressings. Scale bar: 50 μm. (c) SEM images of bacteria on BC/Ag dressings. Scale bars: 1 μm.

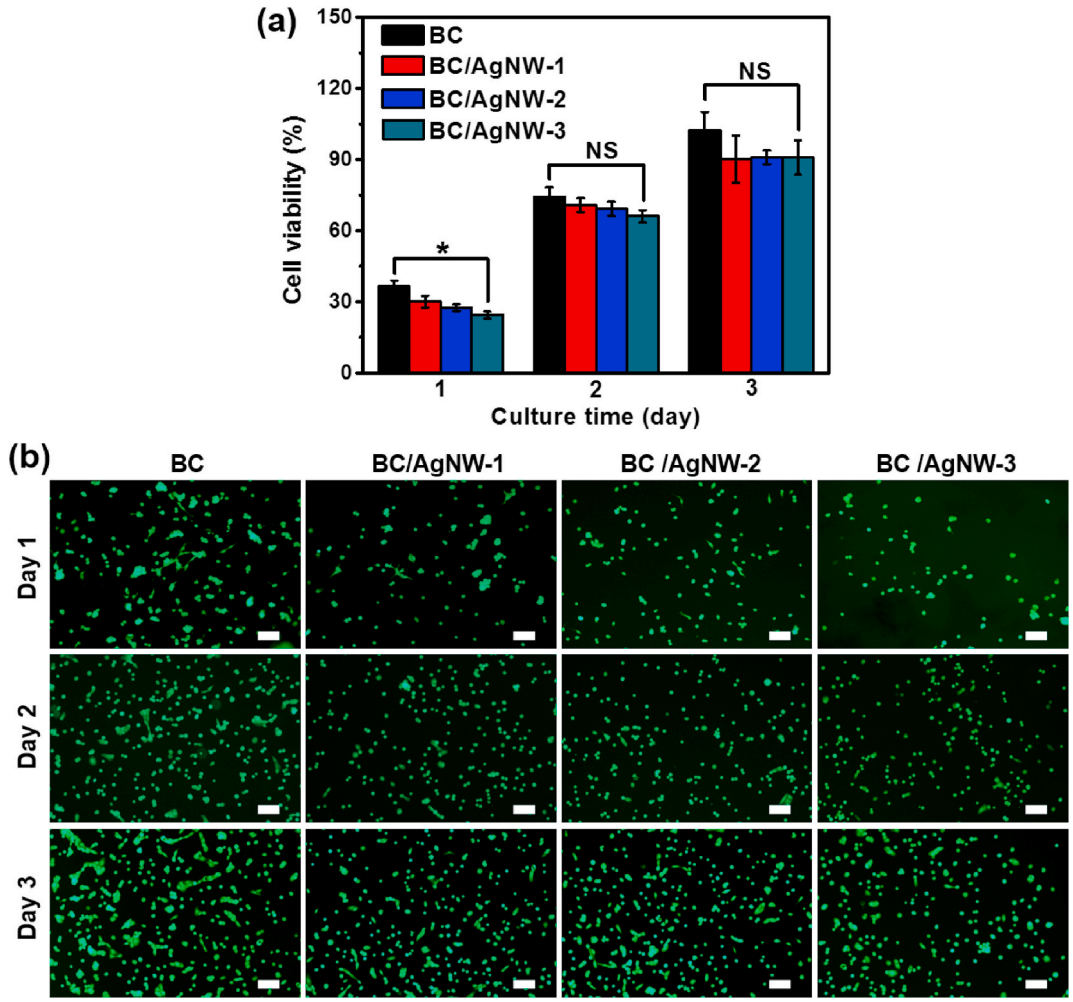

Fig. 7. (a) Viability of NIH-3T3 cells cultured on BC/AgNW dressings. (b) Fluorescent images of NIH-3T3 cells cultured on BC/AgNW dressings. *$p < 0.05$, n = 5. NS means insignificant, $p > 0.05$. Scale bars present 100 μm.

dressings. Therefore, the result further indicates that BC/AgNW dressings show little toxicity, making them suitable materials for wound dressings.

3.4. *In vivo* wound healing

For *in vivo* studies, only BC/AgNW-3 dressing was selected owing to its high AgNWs content and favorable mechanical properties and biocompatibility. The bare BC and BC/AgNW-3 dressings were used in wound healing assays. Wounds without any dressing were used as control. The wounds were monitored for 12 days and their images were photographed at the 3rd, 6th, 9th, and 12th day post operation (Fig. 8a). In addition, the wound healing rate (WHR), which is expressed by the percentage of wound area closure, was evaluated (Fig. 8b). At day 3, BC/AgNW-3 dressing shows a WHR of 28% while it is 10% for bare BC and control groups. Similarly, the BC/AgNW-3 dressing shows higher WHR than bare BC and control groups at days 6 and 9. At day 12, 90% of wound is healed for bare BC and control group whereas the wound is almost completely healed and robust growing hair is noted for the BC/AgNW-3 group, approaching normal healthy skin, suggesting that the BC/AgNW-3 dressing has excellent healing ability.

Histological examination, via HE staining, was conducted to examine the wound healing for up to 12 days (Fig. 9a). At day 3, granulation tissue is observed. In the control and bare BC groups, a large number of inflammatory (inside dotted lines) and infiltrated cells are observed and severe fibrous hyperplasia and disordered tissue structure are observed. Interestingly, in the BC/AgNW-3 group, there are fewer inflammatory cells and orderly tissue structure and abundant granulation tissue are noted. Furthermore, in the BC/AgNW-3 group, the wound is occupied by the epidermal layer at 12th day, and the presence of mature cuticle indicates the re-epithelialization of new skin regeneration. However, in the control and BC groups, the scar tissue is thicker, and the mature cuticle and re-epithelialization are fewer, compared to the BC/AgNW-3 group. Moreover, hair follicle growth (red arrow) is observed in the BC/AgNW-3 group. Therefore, such histology results indicate that the BC/AgNW-3 dressing greatly promotes skin regeneration.

Immunohistochemistry analysis was also performed. Firstly, expression of cytokeratin-10 (CK-10) was determined. To distinguish the keratinizing pathway expressed during wound healing, keratin CK-10, a mature marker, was selected. At day 3, there are a small number of keratinocytes (green) in the BC and control groups, while the BC/AgNW-3 group shows complete and continuous keratinocytes in the epidermis (Fig. 9b). At day 12, there are some proliferated keratinocytes in the epithelial tissues in the control and BC groups, but the structure is not organized. In the BC/AgNW-3 group, proliferation and differentiation of multiple layers of tightly linked keratinocytes are observed, which is very beneficial to the integrity of the basal membrane of the skin. Expression of integrin-β4 was also analyzed (Fig. 9c). Note that the control and BC groups are not completely filled with granulation tissue and proliferative epithelial tissues are not found. In the BC/AgNW-3 group, fully grown epithelial tissues are noted indicating a high degree of healing.

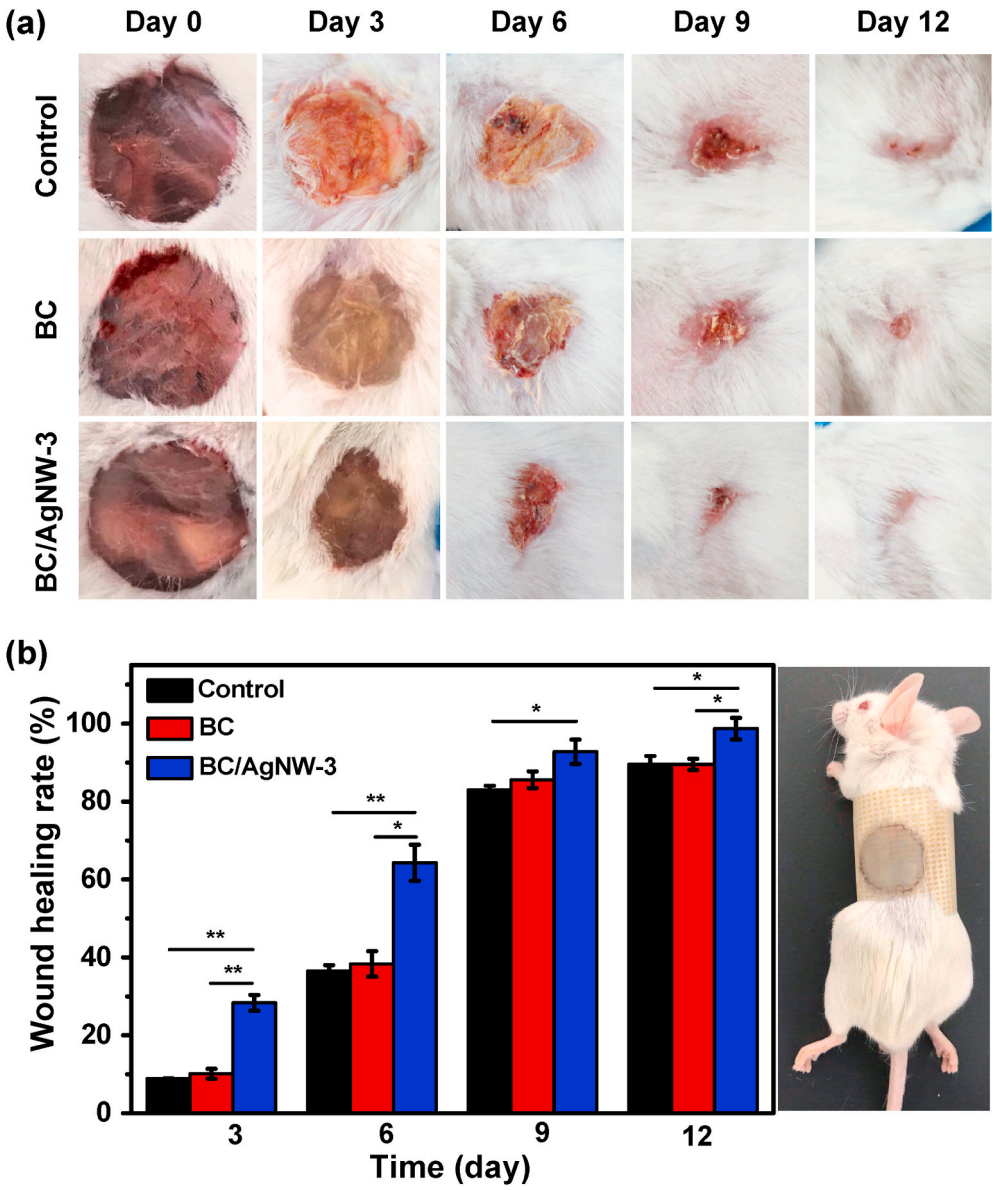

Fig. 8. *In vivo* animal experiment results. (a) Optical images of the wounds at days 3, 6, 9, and 12 after covering with dressings. (b) Wound healing rate (WHR) after covering with dressings.

4. Discussion

Silver has long been used in treating bacterial infections, wounds, burns and cuts largely because of its bactericidal effect. The mechanism of such effect is due to the release of Ag^+ or the generation of reactive oxygen species, or both, which leads to bacterial cell wall disintegration, DNA dimerization, respiratory chains inhibition and ultimately death [43]. Nevertheless, in human being, prolonged exposure to excessive Ag^+ may provoke harmful side effects such as argyria [44]. Furthermore, Ag^+ depletion as a result of fast and successive Ag^+ release may cause reduced bacterial inhibition efficiency [45]. These problems are more severe when nanoparticle-shaped silver is used since its larger surface area than other silver shapes (e.g. wire-shaped silver). In this study, we used AgNWs which not only achieve sustained and excellent antibacterial activity and improved mechanical properties, but also maintain the nanofibrous and highly porous structure of pristine BC.

Firstly, the obtained data in Fig. 5d suggest that the BC/AgNW dressings exhibit almost a constant releasing rate of Ag^+ during the whole process of 9 days. The highest release rate of Ag^+ for BC/AgNW-3 on the 9th day is 160 μg g^{-1}, which is converted to an Ag^+ concentration of 1.5 μg mL^{-1}. This value is comparable to a previously reported safe Ag^+ concentration of 1.77 μg mL^{-1} for A549 lung cells [46]. Such releasing behavior can not only enable the dressings to have sustained release (thus keeping long-term antibacterial activity) but also mitigate any possible cytotoxicity (thus showing good biocompatibility). Moreover, compared to other Ag-loaded dressings, BC/AgNW-3 shows better antibacterial activity. For instance, the BC/AgNW-3 shows inhibition zones of 5.8 mm and 6.5 mm against *E. coli* and *S. aureus*, respectively, which are much larger than those of previously reported AgNP-loaded dressings (Table S2, Supplementary Material) except for polyvinylpyrrolidone-ciprofloxacin/ethyl cellulose-AgNPs that showed an inhibition zone of 8.5 mm against *E. coli* [47].

Secondly, BC/AgNW dressings exhibit interpenetrated structure in which AgNWs and BC nanofibers are entangled together leading to robust dressings. Such characters are important because a qualified wound dressing must be strong and stretchable enough to resist the physical stress and also be soft enough to allow for the patient's daily activities. The mechanical tests do confirm that the incorporation of

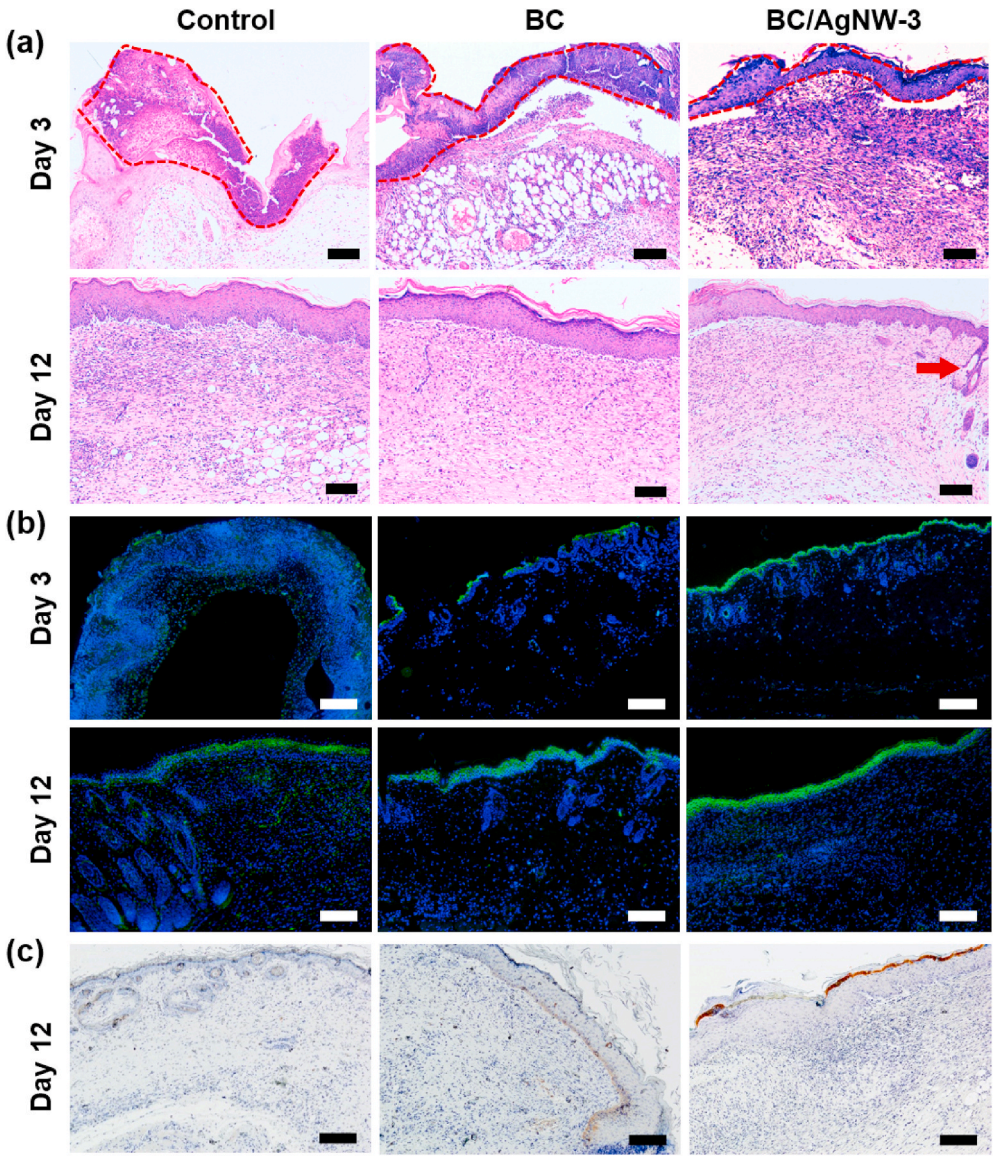

Fig. 9. Staining results of untreated, BC-treated, and BC/AgNW-3-treated wounds. (a) Histological analysis of the wounds 3 and 12 days post operation. The areas inside dotted lines indicate presence of inflammatory cells. (b) Immunofluorescence staining of cytokeratin-10 (CK-10) 3 and 12 days post operation. (c) Immunohistochemical staining of integrin-β4 12 days post operation. Scale bars: 100 μm.

AgNWs endows the BC/AgNW dressings with enhanced mechanical strength (Fig. 4), an important character for clinical use.

Thirdly, the BC/AgNW dressings show highly porous nanofibrous structure (Fig. 2) although the porosity and pore size are relatively smaller than those of bare BC. Such structure provides biophysical cues to promote cell proliferation [48], thus accelerating the wound healing process and promoting wound repair. In addition, the porous structure, together with the hydrophilicity (Fig. S7), endows the BC/AgNW dressings with large water uptake and suitable WVP (Fig. 5).

Besides those physiochemical properties, the biocompatibility of BC/AgNW dressings was tested with *in vitro* experiments including CCK-8 assay and fluorescent microscopy. Results from the *in vitro* experiments suggest that the addition of AgNWs does not have significant impact on cellular responses to the dressings such as cell attachment, growth, and proliferation. These results imply that the incorporation of AgNWs does not cause obvious cytotoxicity.

In vivo experiments with mice were conducted to accurately characterize the processes of wound healing. Digital images and wound healing rate (Fig. 8) clearly show the quicker wound healing in the BC/AgNW-3 group as compared with BC and control groups, which indicates the role of AgNWs in promoting wound healing. Indeed, some previously studies confirmed that silver can quicken the healing rate and stimulate the proliferation and relocation of keratinocytes [49,50]. Furthermore, Liu et al. reported that the silver can improve the proliferation of keratinocytes and trigger the differentiation and maturation of keratinocytes [51]. Our result (Fig. 9b) supports those findings. It is known that cytokeratin is widely distributed in the epidermis in normal skins [52]. In the repairing process of damaged skin, the epidermal differentiation at each stage is characterized by the expression of specific proteins such as keratin-10 [53]. The result in Fig. 9b indicates that the expression of CK-10 in the BC/AgNW-3 group is much higher compared with the control and BC groups, indicating the higher epidermal differentiation degree [52]. Integrin is one of the significant members of cell adhesion molecule family. The integrin β4 mainly mediates the adhesion between cells and ECM components and indicates the skin wound healing degree. Upregulation of integrin β4 expression can promote tight connection between epithelial cells and fibroblasts, and accelerate wound healing [54]. In this study, the higher expression of integrin β4 for the BC/AgNW-3 group than those of the control and BC groups (Fig. 9c) suggests its better and faster recovery of epithelial tissue

[54], which agrees with many previous results [51,55].

All these results suggest that the BC/AgNW dressings exhibit excellent wound healing capability and negligible inflammatory response. The inflammation-free nature is due to its favorable antibacterial properties derived from sustained release of Ag^+. The favorable wound healing capability can be ascribed to the combined effects of porous nanofibrous structure, good hydrophilicity, suitable moist keeping ability and WVP. Results from this study indicate that the BC/AgNW dressings is a suitable wound dressing to effectively prevent infection and accelerate wound healing, which can also be used as an excellent wound coverage material.

5. Conclusions

In summary, BC/AgNW composites have been successfully fabricated as new wound dressings via a novel step-by-step *in situ* biosynthesis. The BC/AgNW dressings display plentiful pores and suitable water vapor permeability, water uptake rate, and water retention rate, which are advantageous for reducing exudates and preserving a humid environment. Moreover, the BC/AgNW dressings show a porous structure with hydrophilic and nano-topographical surface. More importantly, the BC/AgNW dressings show sustained release of Ag^+, which contributes to the long-term excellent antibacterial activities against *E. coli* and *S. aureus* and non-toxicity to NIH-3T3 cells. *In vivo* animal tests reveal that the BC/AgNW dressings display enhanced wound healing ability and a faster re-epithelization and tissue organization as compared with BC and untreated control groups, which are related to the excellent antibacterial activities. These results suggest that the BC/AgNW dressings could be promising wound dressings. In summary, this study presents a simple and effective method for preparing novel BC/AgNW-based dressings for potential medical wound caring purposes.

CRediT authorship contribution statement

Yizao Wan: Funding acquisition, Conceptualization, Methodology, Formal analysis. **Shanshan Yang:** Conceptualization, Methodology, Formal analysis. **Jie Wang:** Conceptualization, Methodology, Formal analysis. **Deqiang Gan:** Investigation. **Miguel Gama:** Writing - review & editing. **Zhiwei Yang:** Supervision. **Yong Zhu:** Data curation, Visualization, Project administration. **Fanglian Yao:** Writing - original draft.

Declaration of competing interest

The authors declare that they have no known competing financial interests or personal relationships that could have appeared to influence the work reported in this paper.

Acknowledgements

Y. Wan, S. Yang, and J. Wang contributed equally to this work, which was funded by the National Natural Science Foundation of China (Grant nos. 31870963, 51973058) and the Provincial Key Research and Development Program of Jiangxi (No. 20192ACB80008).

Appendix A. Supplementary data

Supplementary data to this article can be found online at https://doi.org/10.1016/j.compositesb.2020.108259.

References

[1] Brown AJ. On an acetic ferment which forms cellulose. J Chem Soc 1886;49:432–9.
[2] Picheth GF, Pirich CL, Sierakowski MR, Woehl MA, Sakakibara CN, de Souza CF, et al. Bacterial cellulose in biomedical applications: a review. Int J Biol Macromol 2017;104:97–106.
[3] Ullah H, Santos HA, Khan T. Applications of bacterial cellulose in food, cosmetics and drug delivery. Cellulose 2016;23(4):2291–314.
[4] Stumpf TR, Yang X, Zhang J, Cao X. In situ and ex situ modifications of bacterial cellulose for applications in tissue engineering. Mater Sci Eng C 2018;82:372–83.
[5] Ghaee A, Bagheri-Khoulenjani S, Amir Afshar H, Bogheiri H. Biomimetic nanocomposite scaffolds based on surface modified PCL-nanofibers containing curcumin embedded in chitosan/gelatin for skin regeneration. Compos Part B 2019:177.
[6] Liang L, Hou T, Ouyang Q, Xie L, Zhong S, Li P, et al. Antimicrobial sodium alginate dressing immobilized with polydopamine-silver composite nanospheres. Compos Part B 2020;188:107877.
[7] Ma R, Wang Y, Qi H, Shi C, Wei G, Xiao L, et al. Nanocomposite sponges of sodium alginate/graphene oxide/polyvinyl alcohol as potential wound dressing: in vitro and in vivo evaluation. Compos Part B 2019;167:396–405.
[8] Nešović K, Janković A, Kojić V, Vukašinović-Sekulić M, Perić-Grujić A, Rhee KY, et al. Silver/poly(vinyl alcohol)/chitosan/graphene hydrogels – synthesis, biological and physicochemical properties and silver release kinetics. Compos Part B 2018;154:175–85.
[9] Wang Y, Wang C, Qiao L, Feng J, Zheng Y, Chao Y, et al. Shape-adaptive composite foams with high expansion and absorption used for massive hemorrhage control and irregular wound treatment. Appl Mater Today 2018;13:228–41.
[10] Yang J, Chen Y, Zhao L, Feng Z, Peng K, Wei A, et al. Preparation of a chitosan/carboxymethyl chitosan/AgNPs polyelectrolyte composite physical hydrogel with self-healing ability, antibacterial properties, and good biosafety simultaneously, and its application as a wound dressing. Compos Part B 2020;197:108139.
[11] Czaja W, Krystynowicz A, Bielecki S, Brown RM. Microbial cellulose-the natural power to heal wounds. Biomaterials 2006;27(2):145–51.
[12] Ul-Islam M, Khan T, Khattak WA, Park JK. Bacterial cellulose-MMTs nanoreinforced composite films: novel wound dressing material with antibacterial properties. Cellulose 2013;20(2):589–96.
[13] Wu C, Fuh S, Lin S, Lin Y, Chen H, Liu J, et al. Tempo-oxidized bacterial cellulose pellicle with silver nanoparticles for wound dressing. Biomacromolecules 2018;19(2):544–54.
[14] Wu J, Zheng Y, Wen X, Lin Q, Chen X, Wu Z. Silver nanoparticle/bacterial cellulose gel membranes for antibacterial wound dressing: investigation in vitro and in vivo. Biomed Mater 2014;9(3):035005.
[15] Ye S, Jiang L, Wu J, Su C, Huang C, Liu X, et al. Flexible amoxicillin-grafted bacterial cellulose sponges for wound dressing: in vitro and in vivo evaluation. ACS Appl Mater Interfaces 2018;10(6):5862–70.
[16] Kingkaew J, Kirdponpattara S, Sanchavanakit N, Pavasant P, Phisalaphong M. Effect of molecular weight of chitosan on antimicrobial properties and tissue compatibility of chitosan-impregnated bacterial cellulose films. Biotechnol Bioproc Eng 2014;19(3):534–44.
[17] Gao C, Yan T, Du J, He F, Luo H, Wan Y. Introduction of broad spectrum antibacterial properties to bacterial cellulose nanofibers via immobilising epsilon-polylysine nanocoatings. Food Hydrocolloids 2014;36:204–11.
[18] Maneerung T, Tokura S, Rujiravanit R. Impregnation of silver nanoparticles into bacterial cellulose for antimicrobial wound dressing. Carbohydr Polym 2008;72(1):43–51.
[19] Polivkova M, Strublova V, Hubacek T, Rimpelova S, Svorcik V, Siegel J. Surface characterization and antibacterial response of silver nanowire arrays supported on laser-treated polyethylene naphthalate. Mater Sci Eng C 2017;72:512–8.
[20] Luo H, Xie J, Xiong L, Zhu Y, Yang Z, Wan Y. Fabrication of flexible, ultra-strong, and highly conductive bacterial cellulose-based paper by engineering dispersion of graphene nanosheets. Compos Part B 2019;162:484–90.
[21] Lv P, Zhou H, Zhao M, Li D, Lu K, Wang D, et al. Highly flexible, transparent, and conductive silver nanowire-attached bacterial cellulose conductors. Cellulose 2018;25(6):3189–96.
[22] Luo H, Xiong P, Xie J, Yang Z, Huang Y, Hu J, et al. Uniformly dispersed freestanding carbon nanofiber/graphene electrodes made by a scalable biological method for high-performance flexible supercapacitors. Adv Funct Mater 2018;28:1803075. 0.
[23] Luo H, Dong J, Yao F, Yang Z, Li W, Wang J, et al. Layer-by-layer assembled bacterial cellulose/graphene oxide hydrogels with extremely enhanced mechanical properties. Nano-Micro Lett 2018;10(3):42.
[24] Luo H, Dong J, Xu X, Wang J, Yang Z, Wan Y. Exploring excellent dispersion of graphene nanosheets in three-dimensional bacterial cellulose for ultra-strong nanocomposite hydrogels. Compos Part A 2018;109:290–7.
[25] Luo H, Dong J, Zhang Y, Li G, Guo R, Zuo G, et al. Constructing 3D bacterial cellulose/graphene/polyaniline nanocomposites by novel layer-by-layer in situ culture toward mechanically robust and highly flexible freestanding electrodes for supercapacitors. Chem Eng J 2018;334:1148–58.
[26] Wan YZ, Huang Y, Yuan CD, Raman S, Zhu Y, Jiang HJ, et al. Biomimetic synthesis of hydroxyapatite/bacterial cellulose nanocomposites for biomedical applications. Mater Sci Eng C 2007;27(4):855–64.
[27] Xiong G, Luo H, Zuo G, Ren K, Wan Y. Novel porous graphene oxide and hydroxyapatite nanosheets-reinforced sodium alginate hybrid nanocomposites for medical applications. Mater Char 2015;107:419–25.
[28] Wang Z, Cui Y, Wang J, Yang X, Wu Y, Wang K, et al. The effect of thick fibers and large pores of electrospun poly (ε-caprolactone) vascular grafts on macrophage polarization and arterial regeneration. Biomaterials 2014;35(22):5700–10.
[29] Venkatesan J, Ryu B, Sudha P, Kim S-K. Preparation and characterization of chitosan-carbon nanotube scaffolds for bone tissue engineering. Int J Biol Macromol 2012;50(2):393–402.
[30] Lin W, Lien C, Yeh H, Yu C, Hsu S. Bacterial cellulose and bacterial cellulose-chitosan membranes for wound dressing applications. Carbohydr Polym 2013;94(1):603–11.

[31] Javanbakht S, Namazi H. Doxorubicin loaded carboxymethyl cellulose/graphene quantum dot nanocomposite hydrogel films as a potential anticancer drug delivery system. Mater Sci Eng 2018;87:50–9.
[32] Qu J, Zhao X, Liang Y, Zhang T, Ma PX, Guo B. Antibacterial adhesive injectable hydrogels with rapid self-healing, extensibility and compressibility as wound dressing for joints skin wound healing. Biomaterials 2018;183:185–99.
[33] Lee TW, Lee SE, Jeong YG. Highly effective electromagnetic interference shielding materials based on silver nanowire/cellulose papers. ACS Appl Mater Interfaces 2016;8(20):13123–32.
[34] Kačuráková M, Smith AC, Gidley MJ, Wilson RH. Molecular interactions in bacterial cellulose composites studied by 1D FT-IR and dynamic 2D FT-IR spectroscopy. Carbohydr Res 2002;337(12):1145–53.
[35] Wang Y, Gu F, Ni L, Liang K, Marcus K, Liu S, et al. Easily fabricated and lightweight PPy/PDA/AgNW composites for excellent electromagnetic interference shielding. Nanoscale 2017;9(46):18318–25.
[36] Ma L, Shen X, Ji Z, Zhu G, Zhou H. Ag nanoparticles decorated MnO_2/reduced graphene oxide as advanced electrode materials for supercapacitors. Chem Eng J 2014;252:95–103.
[37] Yang Y, Guo Y, Liu F, Yuan X, Guo Y, Zhang S, et al. Preparation and enhanced visible-light photocatalytic activity of silver deposited graphitic carbon nitride plasmonic photocatalyst. Appl Catal, B 2013;142–143:828–37.
[38] Ma J, Wang K, Zhan M. A comparative study of structure and electromagnetic interference shielding performance for silver nanostructure hybrid polyimide foams. RSC Adv 2015;5(80):65283–96.
[39] Pierotti R, Rouquerol J. Reporting physisorption data for gas/solid systems with special reference to the determination of surface area and porosity. Pure Appl Chem 1985;57(4):603–19.
[40] Akiyode O, Boateng J. Composite biopolymer-based wafer dressings loaded with microbial biosurfactants for potential application in chronic wounds. Compos Sci Technol 2018;10(8):918.
[41] Zhang H, Luo X, Tang H, Zheng M, Huang F. A novel candidate for wound dressing: transparent porous maghemite/cellulose nanocomposite membranes with controlled release of doxorubicin from a simple approach. Mater Sci Eng C 2017;79:84–92.
[42] Feng QL, Wu J, Chen GQ, Cui FZ, Kim TN, Kim JO. A mechanistic study of the antibacterial effect of silver ions on escherichia coli and staphylococcus aureus. J Biomed Mater Res 2000;52(4):662–8.
[43] Feng QL, Wu J, Chen G, Cui F, Kim T, Kim J. A mechanistic study of the antibacterial effect of silver ions on escherichia coli and staphylococcus aureus. J Biomed Mater Res 2000;52(4):662–8.
[44] Jatoi A, Kim L, Ogasawara H, Ni Q. Characterizations and application of CA/ZnO/AgNP composite nanofibers for sustained antibacterial properties. Mater Sci Eng C 2019;105:110077.
[45] Song J, Kim H, Jang Y, Jang J. Enhanced antibacterial activity of silver/polyrhodanine-composite-decorated silica nanoparticles. ACS Appl Mater Interfaces 2013;5(22):11563–8.
[46] Beer C, Foldbjerg R, Hayashi Y, Sutherland DS, Autrup H. Toxicity of silver nanoparticles—nanoparticle or silver ion? Toxicol Lett 2012;208(3):286–92.
[47] Yang J, Wang K, Yu D-G, Yang Y, Bligh SWA, Williams GR. Electrospun Janus nanofibers loaded with a drug and inorganic nanoparticles as an effective antibacterial wound dressing. Mater Sci Eng C 2020:111.
[48] Wei G, Jin Q, Giannobile WV, Ma PX. Nano-fibrous scaffold for controlled delivery of recombinant human PDGF-BB. J Contr Release 2006;112(1):103–10.
[49] Gunasekaran T, Nigusse T, Dhanaraju MD. Silver nanoparticles as real topical bullets for wound healing. J Am Coll Clin Wound Spec 2011;3(4):82–96.
[50] Vijayakumar V, Samal SK, Mohanty S, Nayak SK. Recent advancements in biopolymer and metal nanoparticle-based materials in diabetic wound healing management. Int J Biol Macromol 2019;122:137–48.
[51] Liu X, Lee Py, Ho Cm, Lui VC, Chen Y, Che Cm, et al. Silver nanoparticles mediate differential responses in keratinocytes and fibroblasts during skin wound healing. ChemMedChem 2010;5(3):468–75.
[52] Yang SW, Geng ZJ, Ma K, Sun XY, Fu XB. Comparison of the histological morphology between normal skin and scar tissue. Journal of Huazhong University of Science and Technology Medical sciences = Hua zhong ke ji da xue xue bao Yi xue Ying De wen ban = Huazhong keji daxue xuebao Yixue Yingdewen ban 2016;36(2):265–9.
[53] Goren I, Koehler Y, Aglan A, Pfeilschifter J, Beck K, Frank S. Increase of cystathionine-gamma-lyase (CSE) during late wound repair: hydrogen sulfide triggers cytokeratin 10 expression in keratinocytes. Nitric Oxide-Biol Chem 2019;87:31–42.
[54] Huang R, He Z, Bian Y, Lei Z, Wang H, Long Y, et al. A biomimetic basement membrane substitute based on tri-layered nanofibrous scaffold for skin reconstruction. J Biomed Nanotechnol 2019;15(12):2332–50.
[55] Paladini F, Pollini M. Antimicrobial silver nanoparticles for wound healing application: progress and future trends. Materials 2019;12(16):2540.